Astron. Astrophys. 334, 1136–1144 (1998)

ASTRONOMY AND ASTROPHYSICS

Impact polarization and charge exchange as diagnostics of proton beams

C. Balança and N. Feautrier

DAMAP and URA 812 du CNRS, Observatoire de Paris, F-92195 Meudon Cedex, France

Received 19 November 1997 / Accepted 2 March 1998

Abstract. Linear polarization of the hydrogen Hα line has been observed in solar flares. This polarization is actually explained as induced by anisotropic collisional excitation of the $n = 3$ level by vertical proton beams with an energy of a few keV. At such energies, charge exchange between the proton beam and the local H atoms is important and must be taken into account in the statistical equilibrium equations.

Accurate cross sections for direct excitation and charge exchange of $n = 2$ and 3 levels by 1-100 keV protons are calculated in a two-centre atomic orbital close-coupling method and compared to the available experimental data. The comparision shows a good agreement. Cross sections for excitation of the sublevels gives the alignment of the excited states and the polarization fraction of the Lyman α, Lyman β and Balmer α lines. The profiles of the CaII K line and the Hα line observed during the flares are extremely broad and their interpretation requires the introduction of a macroturbulence velocity. From the calculated differential cross sections, we show that, for the collisional energies considered, the recoil velocity of the H atom after direct excitation gives rise to a macroscopic Doppler broadening that can partially explain the observations.

Combining observations of the wing profiles of the Lyman α and β lines, and observations of the polarization of the Hα line would provide complementary diagnostics of the velocity distribution function of the proton beams.

Key words: atomic processes – Line: profiles – polarization – Sun: flares

1. Introduction

Particles are accelerated in solar flares in a wide range of energies. Electrons are detected through the radio, X-ray and γ-ray emission, or through the enhancement of the visible and UV emission continua produced by their interaction with the solar atmosphere (Vogt & Hénoux 1996). High energy protons produce detectable γ-ray emission by bombarding the solar atmosphere. They are also detected in the interplanetary space. But low energy protons are more difficult to detect.

Send offprint requests to: C. Balanca@obspm.fr

One possible diagnostic is the interpretation of the line profiles. The observed lines are very large and show an enhancement of the red wing (Fang et al. 1995), interpreted as due to the Doppler shifted emission of the neutral H atoms formed by charge exchange. In the line centre, the profile may be broadened by a macroscopic Doppler effect due to the H atom recoil motion after excitation. As shown in the following, this recoil motion may be of the same order of magnitude or larger than the thermal isotropic velocity distribution. The velocity direction of such excited atoms is perpendicular to the velocity of the outgoing protons, the Doppler broadening is thus directly related to the differential excitation cross section.

Another method is the observation of impact linear polarization of atomic lines (Hénoux et al. 1990). Excitation of a set of atoms (or ions) by non isotropic collisions leaves it in an anisotropic state. Light emitted in the subsequent decay manifests this anisotropy through its polarization (Percival & Seaton 1958, Dyakonov 1965, Fano & Macek 1973, Blum 1981). Much attention has been paid to this mechanism, both for excitation by electron beams (Percival & Seaton 1958, Fano & Macek 1973, Blum 1981) or by ionic beams (Carré et al. 1977, Petrashen et al. 1984) in relation with laboratory measurements. Recent observations of solar chromospheric flares (Hénoux et al. 1990, Hénoux 1991) show linearly polarized Hα emission. The observed polarization degree can be as high as 10% for a flare located near the limb and one minute integration time. This polarization can be interpreted as anisotropic collisional excitation of the $n = 3$ level of the H atom by vertical protons beams with initial energies at the coronal level of a few hundred keV, and thus energies of a few keV in the chromosphere.

For a quantitative interpretation of the observed polarization, one needs accurate values of all the collisional and radiative processes for populating and depopulating the Zeeman sublevels of the H atom (Vogt et al. 1997). The radiative contribution due to absorption of the local Lyα, Lyβ and Hα radiation may be easily calculated when the radiation field is known, and thus depends on the model of atmosphere. Two collisional processes are present: firstly excitation from the $n = 1$ level by the beam particles, and secondly collisional transfer of populations and alignment between Zeeman sublevels of the same n level due to local electrons and protons. The latter process has been

correctly evaluated in the semiclassical perturbation approximation (Sahal-Bréchot et al. 1996), but this approximation is no longer valid for excitation by the beam protons, since strong molecular short range interactions are dominant. Furthermore, charge exchange significantly contributes to the excitation for the considered collisional energies and thus must be taken into account. It should be emphasized that excitation by the directive proton beam is the only process giving rise to polarization of the emitted line whereas the other processes all contribute to its depolarization.

To date, only crude values of the excitation cross sections have been used (Vogt et al. 1997). Calculated in a perturbative approach, these cross sections cannot accurately take into account the really important molecular processes occuring in the 0 to 50 keV energy range. Therefore, better cross sections are actually needed. Recently much experimental or theoretical work has been devoted to this problem and new accurate data have become available. However, the partial cross sections for excitation of each magnetic sublevel as well as the differential cross sections, still unknown, are needed to solve the rate equations and to determinate the macroscopic Doppler broadening. In the present work, we have used the most accurate methods, valid in the considered energy range (1-100 keV), to calculate all the relevant integrated and differential cross sections for direct excitation and capture as well as the polarization of the subsequently emitted lines. Sect. 2 briefly outlines the theoretical methods. The results are presented in Sect. 3 and compared to the measurements when available. Astrophysical consequences are discussed in Sect. 4.

2. Description of present H-H$^+$ collision calculations

The two-centre atomic orbital close coupling method (TCAO) (Bates & McCarroll 1958) has been successfully exploited for treating ion-atom collisions in the intermediate energy range (from 1 keV to 200 or 300 keV) over the past two decades. In this energy range, the velocities of the projectile and the active atomic electron are of the same order of magnitude, and thus three reaction processes compete, i.e. excitation, capture and ionization, which makes the TCAO close-coupling method a natural choice to describe the collision process dynamics (Kuang & Lin 1996a).

Within the semi-classical impact parameter approximation, the time dependent wave function $\Psi(\boldsymbol{r},t)$ is expanded in terms of bound atomic orbitals plus continuum states including the plane wave electronic translational factor. The time dependent electronic wave function is given by:

$$\Psi(\mathbf{r},\mathbf{t}) \;=\; \sum_p a_p(t)\phi_p^A(\mathbf{r_A})\;\mathbf{e}^{\mathbf{i}\frac{\mathbf{v}\cdot\mathbf{r}}{\mathbf{2}}-\mathbf{i}\frac{\mathbf{v^2}}{\mathbf{8}}\mathbf{t}-\mathbf{i}\alpha_\mathbf{p}\mathbf{t}} + \sum_q b_q(t)\phi_q^B(\mathbf{r_B})\;\mathbf{e}^{-\mathbf{i}\frac{\mathbf{v}\cdot\mathbf{r}}{\mathbf{2}}-\mathbf{i}\frac{\mathbf{v^2}}{\mathbf{8}}\mathbf{t}-\mathbf{i}\beta_\mathbf{q}\mathbf{t}} \qquad (1)$$

where particle A is the incident proton, i.e. the projectile, and particle B is the proton of the initial hydrogen atom, i.e. the target. $a_p(t)$ and $b_q(t)$ are the transition amplitudes for the occupation of the atomic states $\phi_p^A(\mathbf{r_A})$ and $\phi_q^B(\mathbf{r_B})$ whose respective eigenenergies are α_p and β_q. We have first performed a traditional symmetric TCAO close-coupling calculation (S). The basis set (TCAO-S) includes 26 states on each centre of this symmetric collision, allowing us to describe all the sublevels from $1s$ to $4d_2$. Furthermore it includes other bound states and pseudostates to take the continuum into account.

Fritsch & Lin (1982) have shown that a TCAO calculation with 22 states on each centre reproduces correctly all the first H_2^+ molecular states. However, the TCAO(S) close-coupling method introduces spurious oscillatory structures in the cross sections (Slim & Ermolaev 1994, Kuang & Lin 1996a and b), that are absent in the experimental data (Park et al. 1976, Detleffsen et al. 1994). These structures, due to the representation of the continuum by short range pseudostates, disappear when the basis set includes pseudo-continuum states at only one centre. Thus, to obtain a better agreement for the excitation cross sections and the polarization fraction, we have performed an asymmetric TCAO close-coupling calculation (A), in which all the pseudostates on the projectile centre have been removed. The basis (TCAO-A) includes 26 states on the target centre B and only 19 bound states on the projectile A (Balança et al. 1997). The total cross sections from a state i to a state f are easily obtained for capture and direct excitation:

$$\sigma_{if}^A(E) \;=\; 2\pi\int_0^\infty db\; b\;\mid a_f(b,Z_0)\mid^2$$
$$\sigma_{if}^B(E) \;=\; 2\pi\int_0^\infty db\; b\;\mid b_f(b,Z_0)\mid^2 \qquad (2)$$

The differential cross sections are given by:

$$\frac{d\sigma_{if}(\theta,E)}{d\Omega} = \left|f_{if}^{A,B}(\theta,E)\right|^2 \qquad (3)$$

where the scattering amplitude is:

$$f_{if}^{A,B}(\theta,E) \;=\; m_p v(-i)^{\Delta m+1} \int_0^\infty db\; b\; J_{\Delta m}(\eta b)(T_{if}^{A,B}(b,Z_0)-\delta_{if}) \qquad (4)$$

m_p is the mass of the proton, v the relative velocity, $\Delta m = |m_f - m_i|$ is the difference between the initial and final magnetic quantum numbers, $J_{\Delta m}$ is the Bessel function of integer order Δm, while $\eta = 2m_p v sin(\theta/2)$ and Z_0 is the limit of the integration of the coupled equations ($Z_0 \to \infty$). $T_{if}^{A,B}(b)$ is the transition amplitude from a state i of B to a state j of A or B for an impact parameter b with initial conditions $b_q(b,-\infty) = \delta_{qi}$ and $a_p(b,-\infty) = 0$. The transition amplitude must include the Coulomb phase factor as shown by Dubois et al. (1993). In the case of capture to a state j of A, the amplitude is given by:

$$T_{if}^A(b,Z_0) \;=\; a_f(b,Z_0) \; exp(\frac{i}{v}[2ln(b) - 2ln(\sqrt{Z_0^2+b^2}+Z_0)]) \qquad (5)$$

For direct excitation, the expression is similarly obtained by changing amplitude a_f into b_f. These differential cross sections yields the excited atom angular distribution of velocities. Since the thermal velocities of the hydrogen atoms before excitation

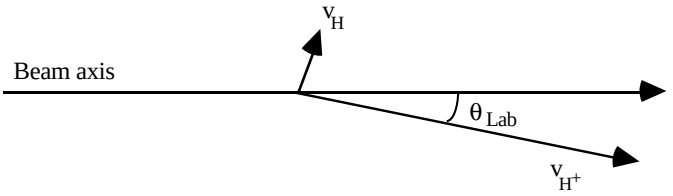

Fig. 1. Diagram of velocities

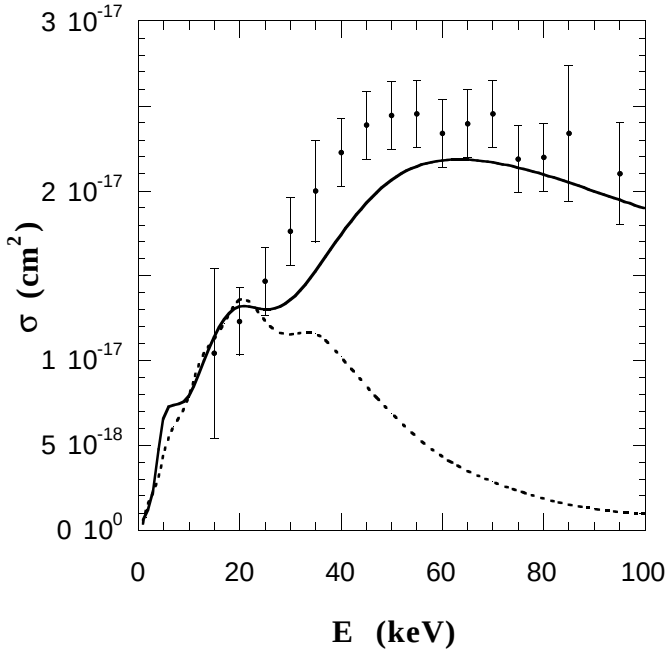

Fig. 2. Total excitation and capture to n=3. Theory: excitation TCAO(A) (full line) and capture TCAO(S) (dotted line). Experiment: excitation • Park et al. 1976.

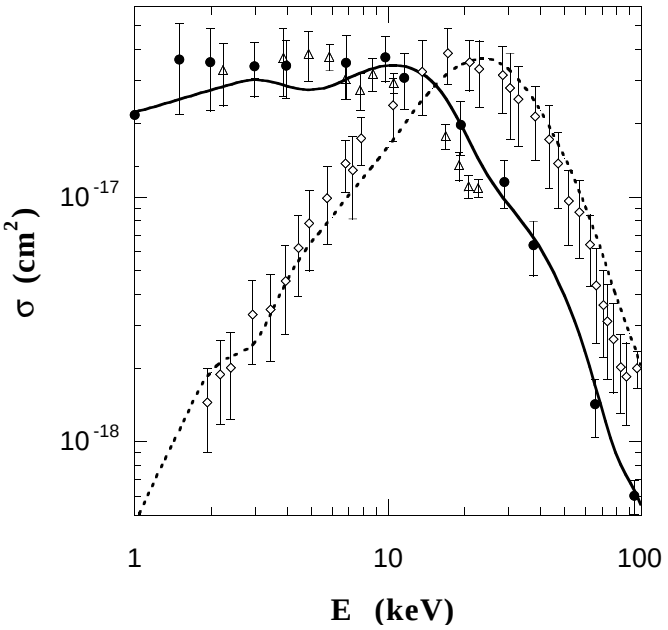

Fig. 3. Capture to n=2. Theory: TCAO(S) 2s (dotted line) and 2p (full line). Experiment: 2s ◇ Morgan et al. 1980, 2p △ Morgan et al. 1973 and • Barnett 1990.

are very small compared to the incoming proton velocities, conservation of the momenta leads us to draw the diagram of the protons and excited atoms velocities as shown in Fig. 1 for direct excitation: the hydrogen atoms move perpendicularly to the direction of the scattered protons. For capture, the relative position of the scattered protons and the excited atoms are exchanged.

3. Results

All the following results have been obtained in a TCAO(A) calculation for the excitation cross sections and a TCAO(S) calculation for the electron capture cross sections, since these approaches are the most accurate in each case, as explained above.

3.1. Excitation and electron capture cross sections to $n = 2$ and 3

Total excitation and electron capture cross sections to $n = 3$ obtained from the present close-coupling calculations are shown in Fig. 2. We would like to point out that the electron capture process is of the same order of magnitude as the direct excitation process for energies lower than 25 keV and that it decreases rapidly when the collision energy E increases. The same behaviour is found for $n = 2$. This is not surprising since for $E \leq 25$ keV, the collision velocity is lower or equal to the classical orbiting electron velocity, which induces equal probabilities for the two processes. For higher energies, the collision is very fast and the capture probability decreases.

In spite of small discrepancies for the lower energies, due to the lack of $l \geq 2$ orbitals in the basis set (Kuang & Lin 1996b), our calculated excitation cross sections are in good agreement with the experimental measurements carried out by Park et al. (1976) and with the more recent theoretical results of Kuang & Lin (1996b). The calculated cross sections for capture and excitation into the $2s$ and $2p$ levels are compared with the available experimental data (Morgan et al. 1973, Morgan et al. 1980 and Barnett 1990 extracted from McLaughlin et al. 1997, Detleffsen et al. 1994 and Higgins et al. 1996) in Figs. 3 and 4. The agreement is good over this energy range. The results for capture and excitation into the $3s$, $3p$ and $3d$ levels are shown in Figs. 5 and 6. The agreement with the experiments is also very good. Nevertheless we want to point out the presence of oscillations in the excitation cross sections around 20 keV partly due to the ionization process which becomes more significant at these energies and must carefully be taken into account. These oscillations would disappear if a larger basis set were used as shown by Kuang & Lin (1996b). This problem does not exist for capture.

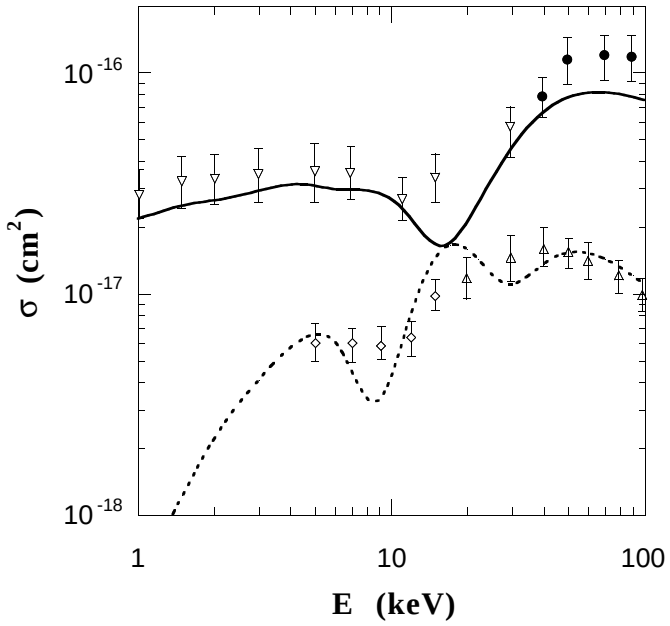

Fig. 4. Direct excitation to n=2. Theory: TCAO(A) 2s (dotted line) and 2p (full line). Experiment: 2s ⋄ Barnett 1990 and △ Higgins et al. 1996, 2p ▽ Barnett 1990 and • Detleffsen et al. 1994.

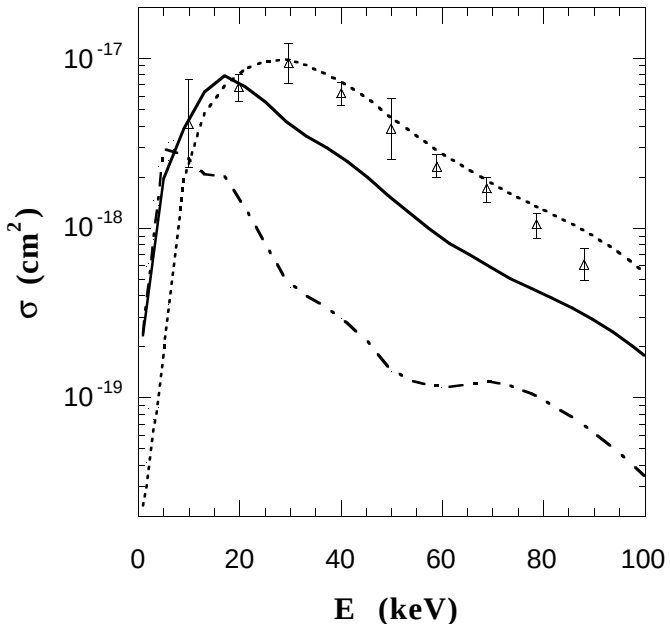

Fig. 5. Capture to n=3. Theory: TCAO(S) 3s (dotted line), 3p (full line) and 3d (broken line). Experiment: 3s △ Hughes et al. 1992.

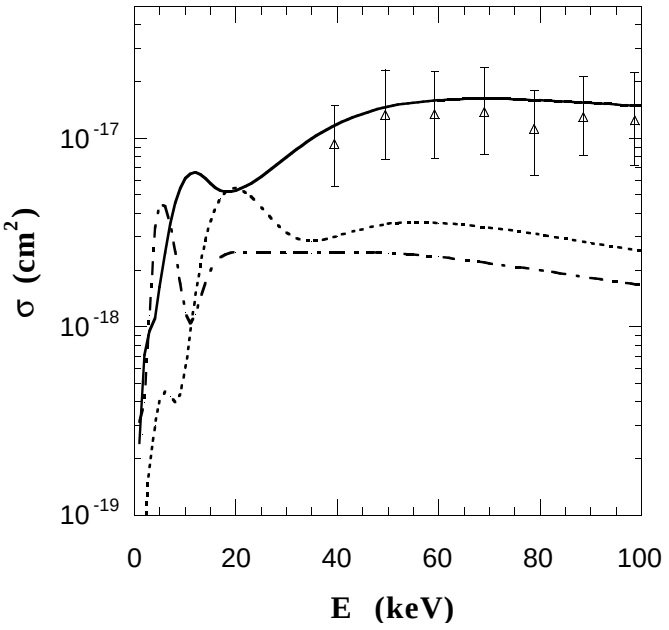

Fig. 6. Excitation to n=3. Theory: TCAO(A) 3s (dotted line), 3p (full line) and 3d (broken line). Experiment: 3p △ Detleffsen et al. 1994.

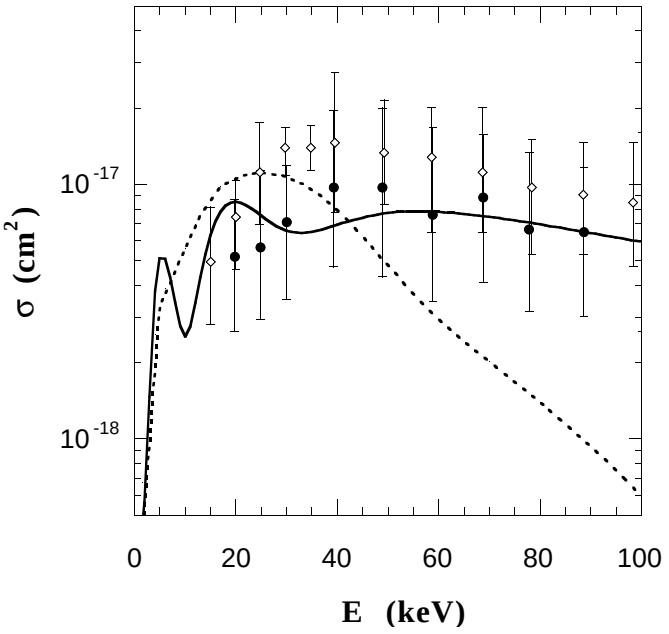

Fig. 7. Balmer Hα cross section. Theory: TCAO(A) Direct excitation (full line), TCAO(S) Capture (dotted line). Experiment: ⋄ Donnelly et al. 1991, • Detleffsen et al. 1994.

3.2. Balmer α emission

The cross section for Balmer α emission, $\sigma(H_\alpha)$, is given by the expression:

$$\sigma(H_\alpha) = \sigma(1s \rightarrow 3s) + 0.1184\sigma(1s \rightarrow 3p) + \sigma(1s \rightarrow 3d) \quad (6)$$

The various $3l$ cross sections coefficients are proportional to the radiative decay to the $n = 2$ level, so that 0.1184 is the branching ratio for the $3p \rightarrow 2s$ decay relative to the $3p \rightarrow 1s$ decay.

In Fig. 7 our results are compared with the available experimental data of Donnelly et al. (1991) and Detleffsen et al. (1994). We note that the data of Donnelly et al. (1991) were not corrected for cascade effects, estimated to be up to 15%. Considering the experimental uncertainties in the Balmer α predictions, there is a satisfactory agreement between our theoretical close cou-

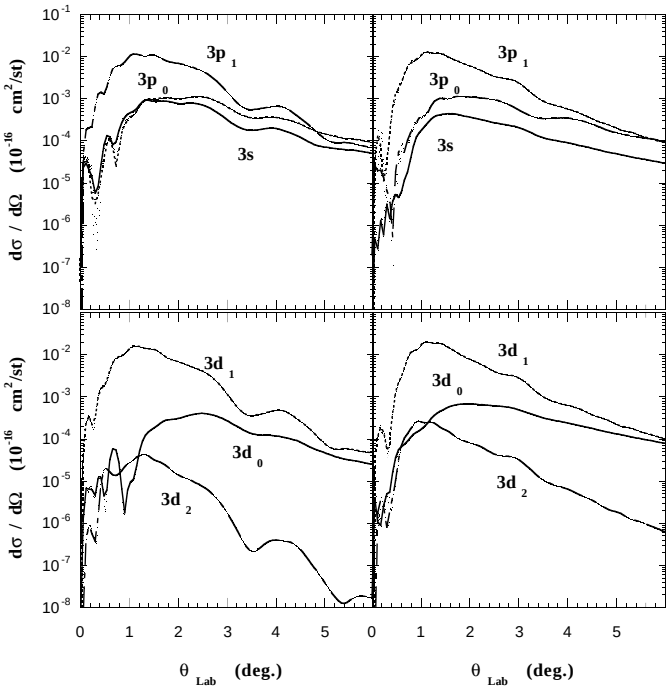

Fig. 8. Reduced differential cross sections $d\sigma/d\Omega = \sin(\theta_{Lab})\, d\sigma_{if}(\theta_{Lab}, E)/d\Omega$ for capture (left) and direct excitation (right).

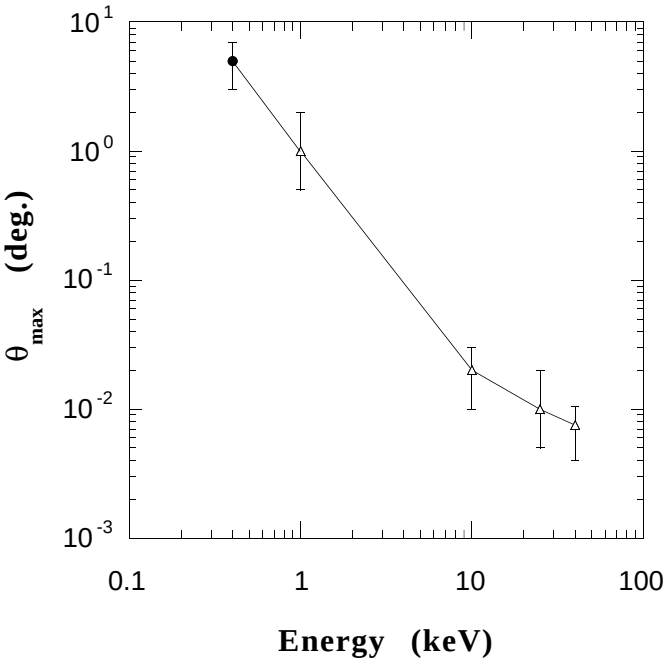

Fig. 9. Variation of θ_{max} versus energy. △ this work; • Gaussorgues & Salin 1971.

pling calculations and the experimental data. Such agreement of the experiment with the close coupling methods was recently pointed out by McLaughlin et al. (1997), who also tested perturbative methods and concluded that the perturbative methods strongly underestimate the cross section for Balmer α emission in the $0-200$ keV energy range. This conclusion justifies the use of close-coupling methods in spite of the large computational effort needed.

3.3. Differential cross sections

Fig. 8 shows for capture and excitation the reduced differential cross sections $d\sigma/d\Omega$= $\sin(\theta_{Lab})d\sigma_{if}(\theta_{Lab}, E)/d\Omega$ of the different sublevels of $n = 3$ for a 1 keV collision energy. All of them are maximum for an angle θ_{Lab} which varies from 10^{-2} to 10^{-1} degree. The reduced differential cross sections for excitation and cature into $n = 2$, not shown here, have a similar behaviour with a maximum for the same angle. This maximum angle θ_{max} varies with energy as shown in Fig. 9. Results for excitation of $n = 2$ at 400 eV (Gaussorgues & Salin 1971) are also reported. One can see that the deflection angle is relatively large at the lowest values of the energy E. Due to the Doppler effect, the intensity of the light emitted in a direction Θ at a given wavelength λ in the near wings of Hα is directly related to the number of excited atoms in a given direction θ_{Lab} from the direction of the incident beam and thus to the differential cross section.

3.4. Polarization fraction of the Lyman α, Lyman β and Balmer α lines

For comparison with the experiments, we consider excitation of unpolarized atoms by unidirectional and monoenergetic protons. Since we are interested in the polarization of radiation emitted from the excited states, the density matrix of these states has to be used. Since the collision duration is small, we assume that the photon is emitted long after the excitation process is completed, so that the excitation and the decay processes can be decoupled. We also consider as negligible the other processes that could modify the statistical equilibrium of the levels. The density matrix of the excited atoms is thus directly related to the scattering amplitudes for excitation of the $i \equiv (n_i l_i m_i)$ magnetic sublevels. If we choose as quantization axis the incident proton beam direction, the density matrix is diagonal and the diagonal elements $\rho(n_i l_i m_i)$ are proportional to the excitation cross sections σ_{gi} from the ground state $g \equiv (n_g l_g m_g)$.

It is useful to introduce the irreducible tensorial representation of the atomic density matrix (Blum 1981):

$$\rho_q^K(n_i l_i) = \sum_{m_i} (-1)^{l_i - m_i} \sqrt{2K+1} \begin{pmatrix} l_i & l_i & K \\ m_i & -m_i & 0 \end{pmatrix} \times \rho(n_i l_i m_i) \quad (7)$$

where the bracket is a (3j) angular momentum recoupling coefficient. The excited atomic states anisotropy can be directly measured by the alignment parameter, proportional to the ρ_0^2/ρ_0^0 ratio (Fano & Macek 1973):

$$A_{20} = \alpha_2 \frac{\rho_0^2}{\rho_0^0} \quad (8)$$

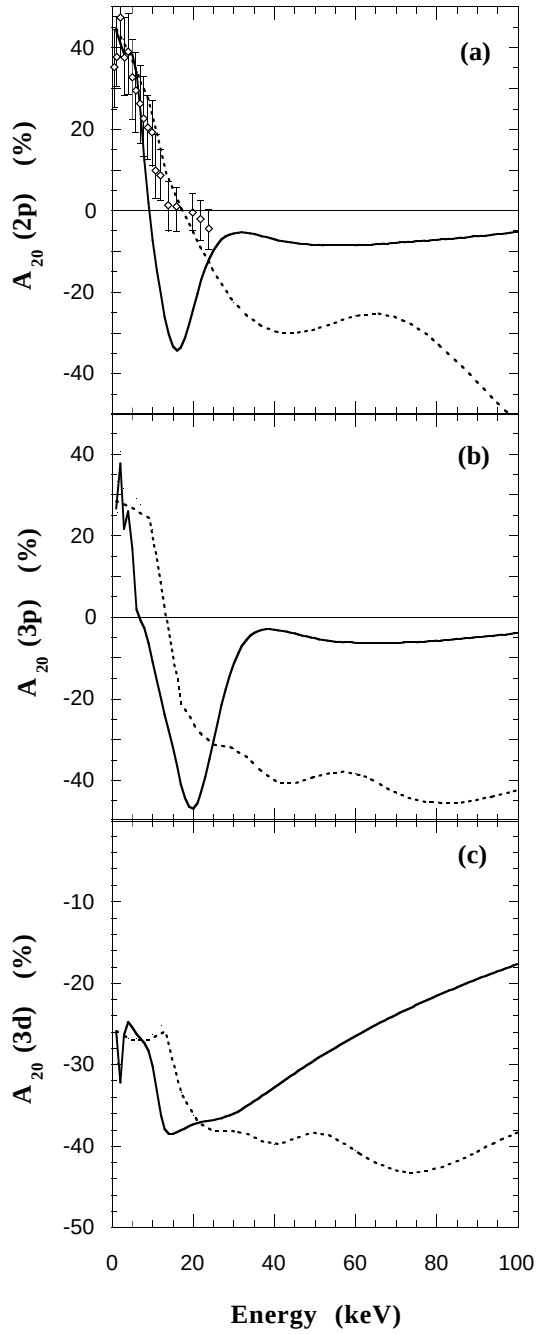

Fig. 10a–c. Alignment A_{20}. Theory: excitation (full line), capture (dotted line). Experiment: ⋄ Hippler 1993.

which depends on the relative population of the $n_i L_i M_i$ magnetic substates. α_2 is defined as:

$$\alpha_2 = (-1)^{l+l'+1}\sqrt{2l+1}\sqrt{\frac{3}{2}}\begin{Bmatrix} 1 & 1 & 2 \\ l & l & l' \end{Bmatrix} \tag{9}$$

for a radiative dipole $nl \rightarrow n'l'$ transition (the brackett is a $\{6j\}$ coefficient). For a $np \rightarrow n's$ transition, A_{20} is given in terms of the cross sections σ_{nlm} for excitation or capture into the sublevel nlm:

$$A_{20} = \frac{\sigma_{np1} - \sigma_{np0}}{\sigma_{np0} + 2\sigma_{np1}} \tag{10}$$

and for a $nd \rightarrow n'p$, A_{20} is given by:

$$A_{20} = \frac{1}{2}\frac{2\sigma_{nd2} - \sigma_{nd1} - \sigma_{nd0}}{\sigma_{nd0} + 2\sigma_{nd1} + 2\sigma_{nd2}} \tag{11}$$

The $2p$, $3p$ and $3d$ levels calculated alignments following excitation and capture by the proton beam are very similar at the lower energies (see Figs. 10 a,b,c respectively), but whereas the negative alignment of the levels excited during a charge exchange process regularly decreases when the energy increases, the alignment of the directly excited levels increases until very small negative value are reached.

Fig. 10a presents our calculated A_{20} compared with the recent experimental data of Hippler (1993) who measured the alignment of the H(2p) level produced either by excitation or by charge transfer. Our results agree with the experimental data, particularly for the lower energies where the alignment is positive. At low incident energies (< 5 keV), A_{20} is close to the maximum value of 50% expected from the rotational coupling theory (Hippler et al. 1988, Hippler (1993)). This result demonstrates that the rotational coupling between the $2p\sigma$ and $2p\pi$ orbitals is the dominant mechanism for H(2p) excitation at these energies: the rotational coupling mechanism only populates the $2p_{\pm 1}$ atomic substates. When the energy increases, the alignment decreases and the mechanisms for H($n = 2$) excitation become more complicated. Direct long range couplings as well as ionization become more important.

The linear polarization degree for observation in the direction Θ from the proton beam direction is defined as:

$$P = \frac{I_{\parallel} - I_{\perp}}{I_{\parallel} + I_{\perp}} \tag{12}$$

where $I_{\parallel}$ ($I_{\perp}$) is the light emissivity when the electric vector is parallel (perpendicular) to the plane defined by the proton beam and the photon travel direction. The emissivities $I_{\parallel} - I_{\perp}$ and $I_{\parallel} + I_{\perp}$ can be written as the sum of the emissivities for each of the $nl \rightarrow n'l'$ transitions which contribute to the line and are expressed in terms of the ρ_0^0 and ρ_0^2 atomic density matrix tensorial elements (Blum 1981):

$$\begin{aligned} I_{\parallel} - I_{\perp} \;=\; & -\sum_{ll'} \frac{h\nu_0}{4\pi} A_{nl\rightarrow n'l'}\sqrt{2l+1} \\ & \times\; \alpha_2 G_2(l)\rho_0^2(l)\frac{3}{2}\sin^2\Theta \end{aligned} \tag{13}$$

$$\begin{aligned} I_{\parallel} + I_{\perp} \;=\; & \sum_{ll'} \frac{h\nu_0}{4\pi} A_{nl\rightarrow n'l'}\sqrt{2l+1} \\ & \times\; (\rho_0^0 + \alpha_2 G_2(l)\rho_0^2(l)\frac{1}{2}(3\cos^2(\Theta - 1))) \end{aligned} \tag{14}$$

$G_2(l)$ accounts for the depolarization due to the fine structure interaction (the hyperfine structure is negligible at the considered densities).

$$G_2(l) = \frac{1}{2S+1} \sum_j (2j+1)^2 \left\{ \begin{array}{ccc} l & j & S \\ j & l & 2 \end{array} \right\}^2 \quad (15)$$

where j denotes a fine structure level of l and $S = \frac{1}{2}$ the atomic spin.

If we introduce P_{90}, the polarization fraction obtained for $\Theta = 90$ degrees, the observed polarization in the direction Θ is given by:

$$P(\Theta) = \frac{P_{90} \sin^2 \Theta}{1 - P_{90} \cos^2 \Theta} \quad (16)$$

Explicit expressions of the polarization fraction P_{90} for the Lyman α, Lyman β and Balmer α lines are the following:

$$\begin{aligned} P_{90}(Ly_\alpha) &= \frac{3(\sigma_{2p0}) - \sigma_{2p1})}{7\sigma_{2p0} + 11\sigma_{2p1}} \\ P_{90}(Ly_\beta) &= \frac{3(\sigma_{3p0} - \sigma_{3p1})}{7\sigma_{3p0} + 11\sigma_{3p1}} \\ P_{90}(H_\alpha) &= (0.1184\frac{\sigma_{3p0} - \sigma_{3p1}}{2} + 57\frac{\sigma_{3d0} + \sigma_{3d1} - \sigma_{3d2}}{100}) \\ &\quad (\sigma_{3s0} + 0.1184\frac{7\sigma_{3p0} + 11\sigma_{3p1}}{6} \\ &\quad + 0.119\sigma_{3d0} + 0.219\sigma_{3d1} + 0.162\sigma_{3d2})^{-1} \quad (17) \end{aligned}$$

The present results for the P_{90} polarization fraction after capture or direct excitation to the $n = 2$ and $n = 3$ levels are shown in Figs. 11 a, b, c. We observe first that P_{90} has the same order of magnitude for the two processes at the lower energies, but decreases much faster with energy for capture than for excitation. However, we want to emphasize that, due to the Doppler shift, the capture and the excitation processes contribute to different regions of the line profile.

The comparison with the available experimental data shows that for Lyman α, our results agree reasonably well with the measurements of Hippler et al. 1988. We also find a good agreement for Hα with the experimental data from Werner & Schartner (1996) obtained at large energies ($E > 40$ keV). At these energies, capture gives no contribution and the experiment yields the polarized emission from directly excited atoms. As for the excitation cross sections (see Sect. 3.1), we note the presence of oscillations in the polarization fraction of the radiation emitted by atoms after direct excitation (without capture). These oscillations, particularly around 20 keV, have no physical significance and a more realistic and smooth polarization fraction variation might be obtained after averaging the calculated values. We want to emphasize that the Hα line polarization fraction is very small for energies larger than 100 keV and indeed recent measurements by Werner & Schartner(1996) have shown that it becomes negative beyond 200 keV.

From the differential cross sections (see Sect. 3.3) we can define a differential polarization fraction giving the polarization of the emitted line due to excited atoms deflected either in direction θ_{Lab} or $\frac{\pi}{2} - \theta_{Lab}$ depending whether capture or direct excitation occurs. Our results (Balança et al. 1997) show that after some oscillations at smaller angles, the polarization fraction is almost constant mainly around the deflection angle maximum.

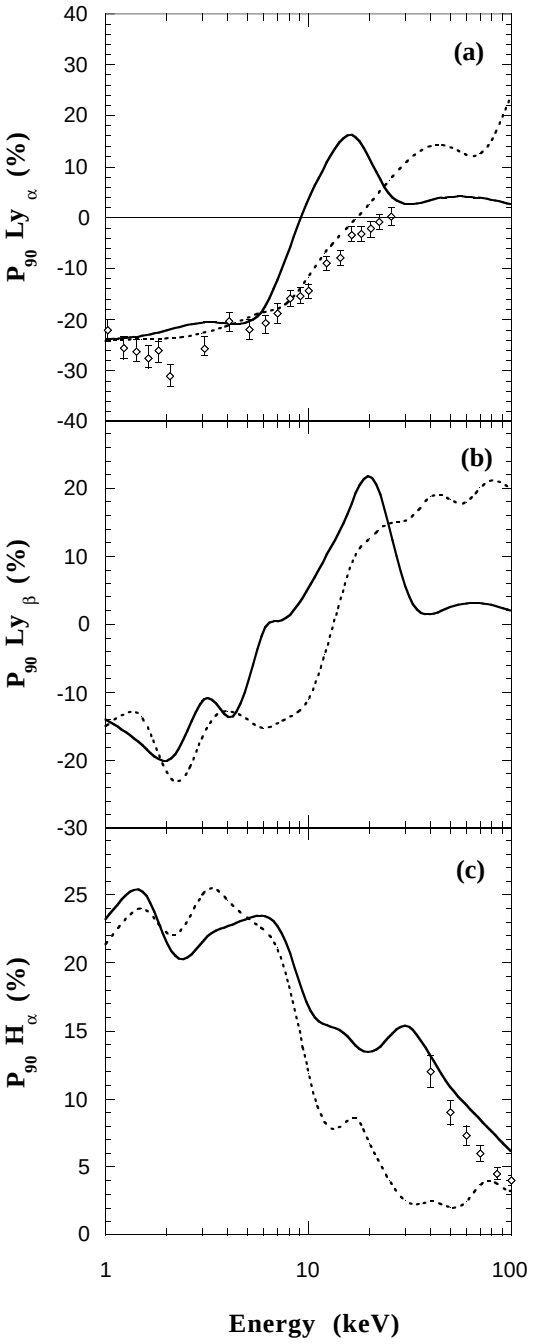

Fig. 11a–c. Polarization as a function of energy **a** $Ly\alpha$, **b** $Ly\beta$ and **c** $H\alpha$. Theory: excitation (full line), capture (dotted line). Experiment: **a** ◇ Hippler et al. 1988 and —bf c ◇ Werner & Schartner 1996.

4. Astrophysical consequences

To date, several diagnostic methods for low energy proton beams have been considered:

- The first one, valid for low energy protons, is based on proton-hydrogen charge exchange. Excitation by a charge exchange process could give rise to very fast hydrogen atoms that produce Doppler shifted emission and consequently enhancements of the line wings of chromospheric lines (Fang et al. 1995).

- The Hα emission enhancement in the line centre and the line central reversal disappearance have been interpreted as due to energy deposition by proton beams in the highest chromosphere layers (Hénoux et al. 1993). But the very large broadening of the lines implies macroscopic velocities whose origin is not clearly explained.

- The third one is based on the proton beams property to keep their anisotropic angular distribution velocity when bombarding the solar chromosphere. The resulting anisotropic collisional atoms excitation generates the emission of a polarized line. Such polarization has been observed during solar flares (Hénoux et al. 1990).

From our results, we can deduce accurate information on these different diagnostic methods which are discussed hereafter.

4.1. Line profiles and Doppler effect

According to the cross sections values, the charge exchange process is important when low energy protons ($E \leq 50$ keV) are present at the chromospheric level. The subsequent Doppler shifted emission has been calculated by Fang et al. (1995) who deduce that, due to the continuum background which is larger by several orders of magnitude, the nonthermal Hα emission would not be detectable. But the nonthermal emission in the red Lyα and Lyβ wings is significantly high and can be used as a diagnostic. The presently calculated cross sections for excitation with charge exchange into the $n = 2$ and $n = 3$ levels agree with the values used by Fang et al. (1995) and we confirm their conclusions. Due to the very fast spontaneous emission process and the low particles density in the chromosphere, charge exchange of the excited atoms with the ambient protons is negligible and consequently no population transfer between fast atoms (excited by charge exchange) and slow atoms (excited directly by the beam) significantly contributes to the statistical populations equilibrium.

Considering the differential excitation cross sections (without capture), we have shown that the protons deflection angle θ_{Lab} can be of the order of a few degrees for the lowest considered energies. Consequently the excited atoms recoil velocity v_r, given by $v_r \simeq v_p \theta_{Lab}$ for incident protons with velocity v_p, is important compared to the thermal velocities: for a 1 keV proton beam and a 1 degree deflection angle, v_r is between 7 and 40 $km.s^{-1}$. This recoil velocity is approximatively perpendicular to the incident protons direction, and according to the line of sight, may produce an important macroscopic broadening of the emitted line.

Of course, for a quantitative interpretation of the observed profilesone would need to account of the angle Θ between the line of sight and the direction of the magnetic field and of the beam pitch angle of the oblique incident proton beam, both for the wings (Zhao et al. 1997) and for the line centre.

4.2. Polarization

Linear Hα line polarization has been observed in solar flares (Hénoux et al. 1990). The observed polarization degree can be as high as 10% for a flare located near the limb, it can be explained as $n = 3$ level anisotropic collisional excitation by vertical proton beams. The observed polarization parallel to the incident proton beam, corresponds to a positive sign of our calculated polarization fraction. For a quantitative comparison between the calculated and the observed polarization, one needs to consider all the processes that contribute to the population equilibrium of the atomic Zeeman sublevels. Apart from the nonthermal excitation by the beam, radiative excitation as well as population collisional transfer by the ambient particles must be taken into account. These two last processes effectively depolarize the line so that excitation by the beam is the only polarizing mechanism. Considering the polarization degree energy variation (see Fig. 11c and Werner & Schartner 1996), we can deduce that, at the chromosphere level, the protons energy is certainely lower than 200 keV and probably less than 50 keV to produce highly polarized lines as were observed. At the same energies, the sign of the polarization fraction for the Lyman α line is negative, and thus simultaneous observation of the Hα and Lyman α polarization would offer a decisive test of the interpretation of such polarization as due to collisional excitation by a proton beam.

It is important to remark that excitation by a neutral beam of electrons and protons with the same velocity (a 50 keV proton has the same velocity as a 30 eV electron) leads to the same conclusion since the polarization fraction of due to electron impact excitation is positive at low energies and becomes negative at 80 eV (Aboudarham et al. 1992) which corresponds to 150 keV protons.

Our calculations show no significant polarization fraction variation as a function of the deflection angle. Consequently no frequency dependence of the polarization is expected in the line centre. In the far wings, formed by nonthermal emission, the emission at a given position λ is directly related to the particle energy in the incident beam (Zhao et al. 1997), thus the polarization fraction frequency dependence should only reflect the beam energy distribution (see Figs. 11 a,b,c). Hα spectropolarimetric observations were performed by Firstova et al. 1996 but the accuracy of these measurements is not sufficient to conclude quantitatively on the proton beam distribution energy. More observations are needed and will be available in the near future with THEMIS.

5. Conclusion

From accurate calculations, we have obtained all the cross sections that characterize excitation of hydrogen atoms by a proton beam in the 1-100 keV range. All these cross sections agree well with the available experimental data.

Excitation with capture is as important as direct excitation at the lowest energies and the capture process characterizes 1-50 keV proton beams. The subsequent Doppler shifted emission yields chromospheric lines wings' enhancement (Fang et al. 1995) and can be used as a diagnostic method.

The directly excited atoms recoil velocity is of the same order of magnitude, or may be larger, than the thermal velocity, and may produce a macroscopic broadening of the emitted line. This nonthermal broadening process is quite general when excitation by a proton beam is dominant and, for example, may explain the Hα line profile in YZ Canis Minoris flare star (Aboudarham & Abada-Simon 1997 - Personal communication).

Comparison between the observed and the calculated Hα polarization fraction allows us to conclude that, at the chromospheric level, the proton beam may have a significant population of protons in the 1-50 keV energy range. A quantitative comparison between the calculated and the observed polarization needs to consider all the polarizing and depolarizing processes in the statistical populations equilibrium, and indeed such work is in progress. More observations are needed, namely for the frequency dependence of the polarization percentage, that will be available in the near future with the solar telescope THEMIS.

Acknowledgements. The authors would like to acknowledge Prof. C.D. Lin for giving them his computer code, Drs. J.C. Hénoux, S. Sahal and A. Spielfiedel for fruitful discussions and the referee for interesting suggestions. The computations were performed on the Convex and Dec Alpha stations of the Computational Centre of Paris Observatory.

References

Aboudarham J., Berrington K., Callaway J. et al., 1992, A&A 262, 302
Balança C., Lin C.D., Feautrier N., 1997, J. Phys. B: At. Mol. Opt. Phys. accepted for publication
Barnett C.F., 1990, Oak Ridge National Laboratory Report N 6086
Bates D.R., McCarroll R., 1958, Proc. R. Soc. 245, 175
Blum K., Density Matrix Theory and Applications: 1981, Plenum Press
Carré M., Gaillard M. L., Lombardi M., 1977, J. Physique 38, 553
Detleffsen D., Anton M., Werner A., Schartner K.-H., 1994, J. Phys. B: At. Mol. Opt. Phys. 27, 4195
Donnelly A., Geddes J. ,Gilbody H.B., 1991, J. Phys. B: At. Mol. Phys. 24, 165
Dubois A., Nielsen S.E., Hansen J.P., 1993, J. Phys. B: At. Mol. Opt. Phys. 26, 705
Dyakonov M.I., 1965, Sov. Phys. JETP 20, 1484
Fang C., Feautrier N., Hénoux J.-C., 1995, A&A 297, 854
Fano U., Macek J.H., 1973, Rev. Mod. Phys. 45, 553
Firstova N.M., Hénoux J.-C., Kazantsev S.A., Bulatov A.V., 1996, Solar Physics 171, 123
Fritsch W., Lin C.D., 1982, Phys. Rev. A 26, 762
Gaussorgues C.,Salin A., 1971, J. Phys. B: At. Mol. Phys. 4, 503
Hénoux J.-C., 1991,in Solar Polarimetry, Proceedings of the Eleventh National Solar Observatory, Sacramento Peek Summer Workshop, p. 285
Hénoux J.-C., Chambe G., Smith D. et al., 1990, ApJS 73, 303
Hénoux J.-C., Fang C., Gan W.Q., 1993, A&A 274, 293
Higgins D.P., Geddes J., Gilbody H.B., 1996, J. Phys. B: At. Mol. Opt. Phys. 29, 1219
Hippler R., 1993, J. Phys. B: At. Mol. Opt. Phys. 23, 1
Hippler R., Madeheim H., Harbich W., Kleinpoppen K., Lutz H.O., 1988, Phys. Rev. A 38, 1662
Hughes M.P., Geddes J., McCullough R.W., Gilbody H.B., 1992, Nucl. Instrum. Methods B 79, 50
Kuang J., Lin C.D., 1996a, J. Phys. B: At. Mol. Opt. Phys. 29, 1207
Kuang J., Lin C.D., 1996b, J. Phys. B: At. Mol. Opt. Phys. 29, 5443
McLaughlin B.M., Winter T.G., McCann J.F., 1997, J. Phys. B: At. Mol. Opt. Phys. 30, 1043
Morgan T.J., Stone J., Mayo R., 1980, Phys. Rev. A 22, 1460
Morgan T.J., Geddes J., Gilbody H.B., 1973, J. Phys. B: Atom. Molec. Phys. 6, 2118
Park J.T., Aldag J.E., George J.M., Peacher J.L., 1976, Phys. Rev. A 14, 608
Petrashen A.G., Rebane V.N., Rebane T.K., 1984, Sov. Phys. JETP 60, 84
Percival I.C., Seaton M.J., 1958, Phil. Trans. Roy. Soc. London A 251, 113
Slim H.A., Ermolaev A.M., 1994, J. Phys. B: At. Mol. Opt. Phys. 27, L203
Sahal-Bréchot S., Vogt E., Thoraval S., Diedhiou I., 1996, A&A 309, 317
Vogt E., Hénoux J.-C., 1996, Solar Physics 164, 345
Vogt E., Sahal-Bréchot S., Hénoux J.-C., 1997, A&A 324, 1211
Werner A., Schartner K-H., 1996, J. Phys. B: At. Mol. Opt. Phys. 29,125
Zhao X., Fang C., Hénoux J.-C., 1997, A&A accepted for publication